The Impact of Formate-Based Electrolytes on The Electrochemical Performance of Asymmetric Supercapacitors Containing Activated Carbon and MnO 2 as Electrode Materials

Siqi Liu, Camille Douard, Thierry Brousse, Andrea Balducci

The impact of formate-based electrolytes on the electrochemical performance of asymmetric supercapacitors containing activated carbon and MnO_2 as electrode materials

Siqi Liu[1], Camille Douard[2,3], Thierry Brousse[2,3], Andrea Balducci[z,1]

[1] *Friedrich-Schiller-University Jena, Institute of Technical Chemistry and Environmental Chemistry and Center for Energy and Environmental Chemistry Jena (CEEC Jena), Philosophenweg 7a, 07743, Jena, Germany*
[2] *Nantes Université, CNRS, Institut des Matériaux de Nantes Jean Rouxel (IMN), 2 rue de la Houssinière, 44322 Nantes, France*
[3] *Réseau sur le Stockage Electrochimique de l'Energie (RS2E), CNRS FR 3459, 33 rue Saint Leu, 80039 Amiens Cedex, France*

[z]*Corresponding author: andrea.balducci@uni-jena.de*

Abstract

In this work we report on the properties of three novel aqueous electrolytes containing 1 m (mol kg^{-1}) of lithium formate, sodium formate and potassium formate in H_2O. We show that these cheap and environmentally friendly electrolytes display high conductivity and low viscosity from 0°C to 80°C. When used in asymmetric supercapacitors (SCs) containing Manganese dioxide (MnO_2) as active material in the positive electrode and activated carbon (AC) as active material in the negative electrode, these electrolytes allow the design of devices with operating voltage up to 1.7 V. Asymmetric SC containing these novel electrolytes display good capacity (19 mAh g^{-1}, 18 mAh g^{-1} and 13 mAh g^{-1} in 1 m HCOOK in H_2O, 1 m HCOOLi in H_2O and 1 m HCOONa in H_2O, respectively). The capacity retention after 10,000 cycles of the devices containing 1 m HCOOLi in H_2O, 1 m HCOONa in H_2O and 1 m HCOOK in H_2O are all higher than 85%.

Keywords

Supercapacitor, Asymmetric device, MnO_2, Aqueous electrolyte, alkaline formates

Introduction

The use of renewable energy sources, e.g., sun and wind, is fundamental to fully replace, or at least dramatically decrease, the dependence of our society on fossil fuels and, at the same time, to reduce the CO_2 emission. However, in order to fully take advantage of these renewable sources, the use of energy storage devices is essential, as it is needed to build up grid-scale storage which can support stable and cost-saving energy supply.[1] Lithium-ion batteries (LIBs) and supercapacitors (SCs) are nowadays among the most important and widely used energy storage devices and their market has been constantly increasing in the last years.[2-6]

SCs can be realized using either activated carbon (AC) based electrodes, in which the energy is physically stored at the electrode/electrolyte interface (double layer capacitance), or pseudocapacitive materials, *e.g.*, RuO_2[7-9] or MnO_2[10-12], in which the energy is stored through fast and reversible faradaic reactions that provide to the electrode a capacitive-like signature[13, 14]. Devices containing both types of electrodes, which are defined as asymmetric, have been also investigated in the past.[15-17]

Among the various pseudocapacitive materials, MnO_2 appears as one of the most interesting due to its high capacitance, high abundance, and environmental friendliness. In the past, a variety of crystal structures of manganese oxide have been investigated, and it has been shown that the type of structure of this oxide has a strong influence on its electrochemical behaviour[18-20] On the other hand, less efforts have been dedicated to the investigation of the impact of the electrolyte on the electrochemical performance of MnO_2. Most of available studies have been carried out using aqueous electrolytes containing KCl, K_2SO_4 or Na_2SO_4. [11,12,15-20,21, 22]

Recently we showed that electrolytes based of potassium formate, *i.e.* which is a cheap, environmentally friendly and non-toxic salt, can be successfully utilized for the realization of high voltage aqueous electrochemical double layer capacitors (EDLCs) displaying high performance and exceptional cycling stability.[23] Taking these results into account, this electrolyte appears very interesting for SC application. However, to the best of our knowledge, a detailed study about the use of formate-based electrolytes in combination with pseudocapacitive materials has not been carried out so far.

In this work, we report on the use of aqueous electrolytes containing lithium, sodium and potassium formate in asymmetric supercapacitors containing AC as negative electrode and MnO_2 as the positive one. Initially, the chemical and physical properties of these electrolytes are considered. In the second part of the manuscript the electrochemical performance of asymmetric SCs containing these electrolytes is investigated in detail.

Experiment

1. Electrolytes characterization

Electrolytes containing 1 m HCOOLi (*Sigma-Aldrich*) in H_2O, 1 m HCOONa (*Sigma-Aldrich*) in H_2O, and 1 m and HCOOK (*Sigma-Aldrich*) in H_2O have been prepared by dissolving the formate salt in deionized water at room temperature according to the molality (molar of dissolved salt in 1 kg solvent.)

The conductivity, viscosity and density of the investigated electrolytes have been measured from 0°C to 80°C. For conductivity measurements, 300 µl of electrolyte was filled in a conductivity cell (MM HTCC-1, *Materials Mates Italia s.r.l*), which was connected to Modulab XM ECS potentiostat (*Solartron*) in a climatic chamber (*Binder*). Then, electrolyte resistance was determined by electrochemical impedance spectroscopy with a frequency scan from 1 Hz to 300 kHz with amplitude of 5 mV, which was carried out as in Ref.[24]. 300 µL electrolyte was used for each viscosity measurement, which was measured by a rotational test with Rheometer MCR 102 (*Perkin Elmer*) as reported in Ref.[24]. In this measurement, the shear rate 1000 s^{-1} was set to measure the shear stress. The system DMA 4000 (*Anton Paar*) was utilized to measure the density. 1.1 mL of electrolyte was consumed for each measurement, which followed the some protocol as in Ref.[25].

2. Electrochemical measurement

Swagelok T type cells made of PFA (Perfluoralkoxy) were used to carry out all the electrochemical measurements. Whatman GF/D glass microfiber filters (675 mm thickness) was utilized as separator between electrodes and soaked with 200 µL electrolyte.

Commercially available α-MnO_2 cryptomelane-type manganese dioxide, MnO_2 H.S.A. (high surface area), was supplied by Prince Corporation (*Baltimore*, MD, USA). The positive electrode contained 60 wt.% MnO_2, 30 wt.% Super C65 (*Imerys*) and 10 wt.% polytetrafluoroethylene (PTFE) (*Sigma Aldrich)*. The negative electrode contained 85 wt.% activated carbon (AC) YP 50F (*Kuraray*), 10 wt.% Super C65 (*Imerys*), and 5 wt.% polytetrafluoroethylene (PTFE) (*Sigma Aldrich*). All electrodes were free standing with stainless steel gird (*SAULAS*) as current collector. They were prepared by mixing the electrode components with ethanol and, after mixing for 1 hour with a magnetic stirrer at 60°C, a slurry was obtained. Afterwards, the electrode slurry was flattened by rolling with a glass rod with the thickness from 35 µm to 300 µm, and then punched into 12 mm diameter round electrode. After drying in the room temperature overnight, the mass loading of the electrodes ranged from 7.1 to 27 mg cm^{-2}.

The performance and the operating voltage of MnO_2 and AC electrode was initially investigated individually in a half cell configuration, in which an oversize counter electrode (AC electrode of ca. 27 mg cm^{-2} and 300 µm thickness) was used. A silver wire was used as pseudo reference electrode. During the experiments, the electrode

potential window was progressively shifted from open circuit voltage toward positive (for MnO_2) or negative (for AC) potential in step of 0.1 V.

The full cells were assembled with MnO_2 electrode as positive electrode, and AC electrode as negative electrode with a mass ratio of MnO_2/AC equal to 1.65:1. This ratio is the result of mass balance process. The mass of positive electrode and negative electrode was balanced according to equation (1) where $m+$ and $m-$ are the mass of active material on positive electrode and negative electrode, respectively. C is the specific capacitance, ΔE is the potential range for the charge/ discharge process.[17]

$$\frac{m+}{m-} = \frac{C-*\Delta E-}{C+*\Delta E+} \qquad \textit{Equation 1}$$

This mass balance was selected taking into account the results of previous investigations of the suitable potential window for each electrode.[17] The operating voltage (OPV) was determined by applying cycling voltammetry (CV) to the full device with scan rate 1 mV s^{-1}.

Initially, the electrochemical performance of the devices was investigated using CV carried out at 1 mV s^{-1}, starting from 0 V and using increasing upper cut-off voltages of 0.8 V, 1 V, 1.4 V and 1.7 V. Then the full cells were cycled utilizing an operating voltage of 1.7 V using scan rate of 1 mV s^{-1}, 2 mV s^{-1}, 5 mV s^{-1}, 10 mV s^{-1}, 20 mV s^{-1} and 50 mV s^{-1}. Galvanostatic charge-discharge were carried out from 0 to 1.7 V using current densities of 0.1 A g^{-1}, 0.2 A g^{-1}, 1 A g^{-1}, 2 A g^{-1}. 100 cycles were carried out under each current density. The long-term cycling stability of devices was investigated by cycling the devices for 10,000 cycles under 1 A g^{-1}. The Impedance spectra were measured with 10 mV ac perturbation in the frequency region from 100 kHz to 10 mHz.

The specific capacitance C (F g^{-1}), specific capacity Q (mAh g^{-1}), coulombic efficiency, energy and power densities of the devices were calculated as reported in reference[26-30]. It must be noted anyway that whenever, a constant capacitance cannot be calculated from the CV or GCD plots, the capacity is reported instead. When the shapes of CVs or GCD only slightly differ from box-type shape and triangular shape respectively, standard calculation for the capacitance were performed.[31]

Results and Discussion

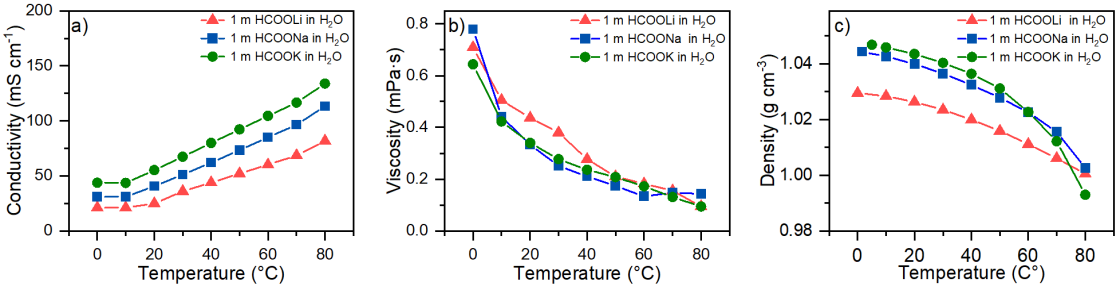

Figure 1. Variation of a) conductivity b) viscosity and c) density of the investigated electrolytes between 0 to 80°C.

Figure 1 compares the temperature dependence of conductivities (Fig. 1a), viscosities (Fig. 1b) and densities (Fig. 1c) of the three electrolytes, namely 1 m HCOOLi, 1 m HCOONa and 1 m HCOOK in H_2O. At 20°C, all electrolytes display high conductivities (25 mS cm^{-1}, 40.8 mS cm^{-1}, 55.3 mS cm^{-1} for 1 m HCOOLi, 1 m HCOONa and 1 m HCOOK in H_2O, respectively), which increase with the temperature. Among the electrolytes, 1 m HCOOK in H_2O is the one displaying the highest conductivity through all the investigated temperature range. This behaviour can be explained by the fact that, although the Shannon's ionic radii of K^+ is the highest among the investigated cations, the hydrated ionic size of K^+ is the smallest, which leads to a better mobility of K^+ in water-based solutions compared to solvated Li^+ and Na^+ (see Table S1 in SI). The viscosities of the electrolytes are rather comparable all over the investigated temperature range. At 20°C it is equal to 0.44 mPa·s, 0.33 mPa·s, 0.34 mPa·s for 1 m HCOOLi, 1 m HCOONa and 1 m HCOOK in H_2O, respectively (see Fig. 1b). The densities of the electrolytes are also comparable, although below 70°C that of 1 m HCOOLi solution is slightly lower than that of the two other electrolytes (1.026 g cm^{-3}, 1.0399 g cm^{-3}, 1.0435 g cm^{-3} for 1 m HCOOLi, 1 m HCOONa and 1 m HCOOK in H_2O at 20°C). This difference is most likely related to the fact that molecular weight of lithium formate is significantly lower than that of the sodium and potassium formates. Taking these results into account, all the investigated electrolytic solutions are displaying properties suitable for their use as electrolytes in aqueous-based SCs.

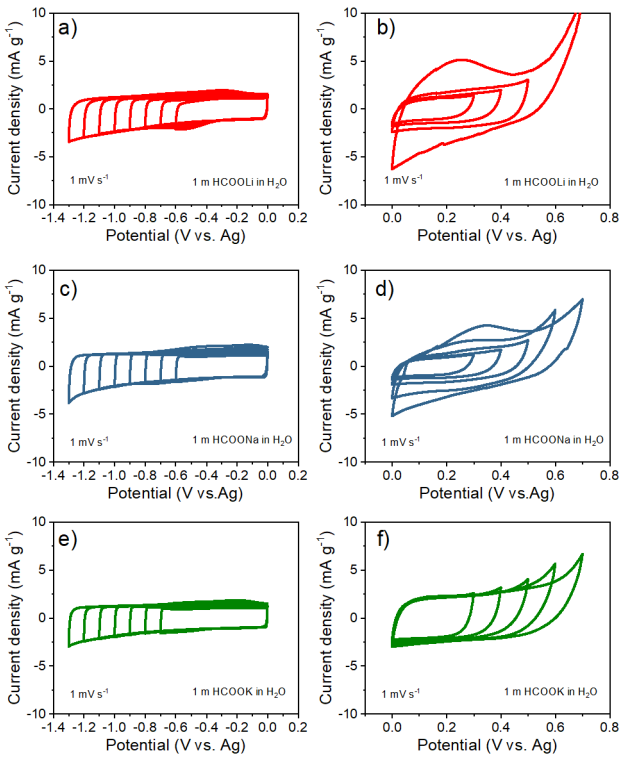

Figure 2. Cyclic voltammogram at 1 mV s^{-1}: a) AC electrode in 1 m HCOOLi in H_2O; b) MnO_2 electrode in 1 m HCOOLi in H_2O; c) AC electrode in 1 m HCOONa in H_2O; d) MnO_2 electrode in 1 m HCOONa in H_2O with MnO_2; e) AC electrode in 1 m HCOOK in H_2O; f) MnO_2 electrode in 1 m HCOOK in H_2O.

Figure 2 is showing the voltametric profiles displayed by AC and MnO_2 electrodes in the investigated electrolytes when different operating potential ranges were applied. These tests have been carried out to determine the operating voltage (OPV) of the asymmetric SCs that will be considered in the following. As shown in the figure (Fig. 2a, c, e), in all electrolytes the AC electrodes display the typical rectangular shape signature between the open circuit potential (OCP) and -1.2 V vs. Ag. At the AC electrode, double layer capacitance is the major charge storage process. During charging process at the negative electrode, cations are adsorbed on the surface of AC electrode with potential sweeping toward negative side. Since cations are solvated by water molecules, continuously water molecules accumulate at negative electrode. Subsequently, a weak reduction peak is observed as an indication of hydrogen adsorption at surface of electrode material. However, no hydrogen evolution seems to occur as demonstrated by OPV float tests shown in Fig. S1 in SI. The leakage current increases at first and then decreases indicating the adsorption process. Upon subsequent oxidation potential scan, the adsorbed hydrogen is reversibly oxidized back to H^+. Such behaviour has already been documented by Béguin et al.[32, 33]. Thus, reversible hydrogen formation/decomposition accounts for a small but measurable part of the charge storage, together with double layer formation. If the potential limit is pushed toward more reductive potential, another reduction peak is observed at over -1.2 V vs. Ag. This peak is related to hydrogen evolution reaction, leading to the decomposition of the electrolyte. Subsequently, the safe potential window for the negative electrode in the formate-based electrolytes must be kept between 0V and -1.2V vs Ag. In this potential window the capacitance values are rather comparable whatever the electrolyte.

In the case of the MnO_2 electrodes the situation is different (see Fig. 2b, d, f). In these electrodes, adsorption and fast surface redox reaction (Equation 2 and 3) are involved in the charge storage mechanism, where C^+ is the proton or an alkaline cation (Li^+, Na^+ or K^+).[11, 12]

$$(MnO_2)_{surface} + xC^+ + xe^- \Leftrightarrow (MnO_2)C_{x_{surface}} \qquad \textit{Equation 2}$$

$$(MnO_2)_{bulk} + yC^+ + ye^- \Leftrightarrow (MnO_2)C_{y_{bulk}} \qquad \textit{Equation 3}$$

As shown, till 0.5 V vs. Ag all electrodes are displaying a rectangular shape, indicating the occurrence of equation (2). However, the electrochemical signature of the electrode is significantly different depending on the electrolyte. In the case of HCOOLi and HCOONa, a pair of redox peaks is superimposed to the box-type shape envelope, thus suggesting that reaction (3) occurs, with bulk intercalation of alkaline cations in the α-MnO_2 tunnels, as it was already reported with other electrolytes.[34]

Among the investigated MnO_2 electrodes, those cycled in 1 m HCOOK in H_2O display higher reversibility and higher capacity of 19 mAh g^{-1} (34 F g^{-1}), while 18 mAh g^{-1} (27 F g^{-1}) and 13 mAh g^{-1} (26 F g^{-1}) where observed in 1 m HCOOLi in H_2O and 1 m HCOONa in H_2O, respectively. Above 0.5 V vs. Ag, oxygen evolution reaction is taking place as indicated by the presence of an increase of oxidative current which is not reversible. It can be noticed that also in this case the increase of this oxidation peak is weaker in the case of HCOOK electrolyte. It must be mentioned that the capacitance and capacity of the investigated electrodes could be further improved by tailoring the MnO_2 polymorph and its morphology for its use in formate-based electrolytes. Nonetheless, this optimization is out of the scope of this study and, therefore, it will not be considered in the following. Taking these results into account, the positive potential limit (for MnO_2 electrode) was fixed to 0.5 V vs. Ag, while that of the negative potential limit (for AC electrode) was fixed to -1.2 V vs. Ag. This leads to the assembly of an asymmetric SC having an operating voltage of 1.7 V. This latter value was used for all three investigated electrolytes.

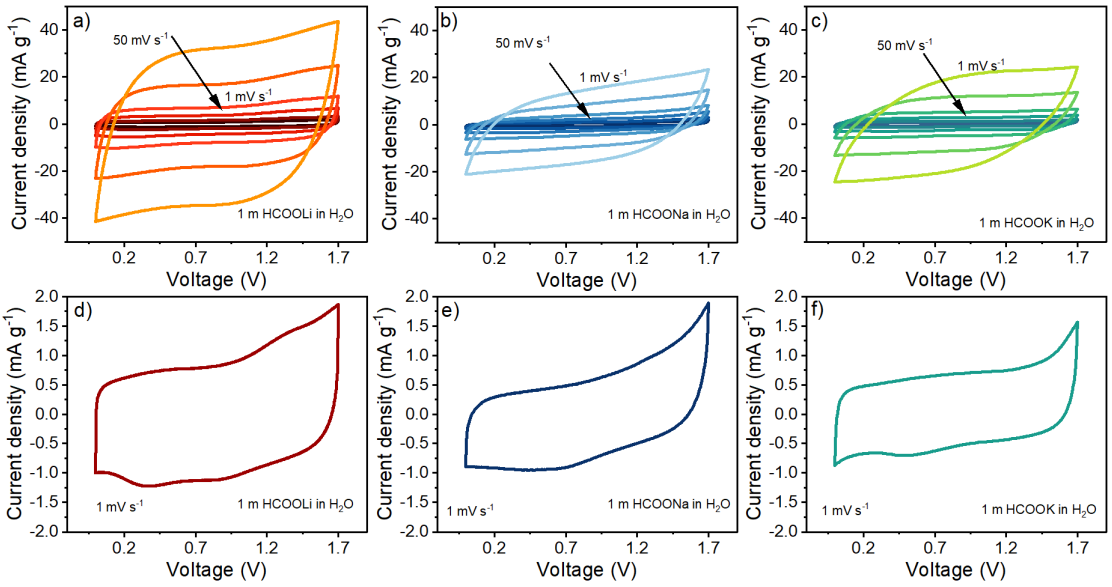

Figure 3. CV of the cells containing a) and d) 1 m HCOOLi in H_2O; b) and e) 1 m HCOONa in H_2O; c) and f) 1m HCOOK in H_2O CV at scan rates of 1 mV s^{-1}, 2 mV s^{-1}, 5 mV s^{-1}, 10 mV s^{-1}, 20 mV s^{-1} and 50 mV s^{-1}.

Figure 3 depicts the CVs of the asymmetric SCs containing the three investigated formate-based electrolytes. As shown, their electrochemical signatures are affected by the used electrolyte. The device containing 1 m HCOOLi in H_2O displays the highest average capacity (referred to the total electrode mass) with 13 mAh g^{-1} (capacitance of 31 F g^{-1}) at 50 mV s^{-1} and a good capacity retention at higher scan rates. The device containing 1 m HCOONa in H_2O, on the other hand, displays lower capacity and a much more distorted plot at high voltage (above 1.5 V). The capacity retention at high

scan rate of this device is also lower compared to that of the device containing HCOOLi. The devices containing HCOOK in H_2O display a more reversible capacitive-like behaviour (although this results from a combination of double layer capacitance on the negative electrode and pseudocapacitance on the positive one) up to 20 mV s^{-1}. It displays a lower capacity compared to the system containing HCOOLi, but its voltammetric profiles are much less distorted than those of the device containing HCOONa. It must be noted that the behaviour of the devices can be affected by their electrode balancing, which might not be the optimal for all electrolytes and for all the tested scan rates. Nonetheless, all devices display fair electrochemical performance and, for this reason, the mass balancing has been kept the same for all the following tests.

To gain insight about the energy and power densities of the investigated devices, galvanostatic charge-discharge cycles were carried out utilizing current densities ranging from 0.1 A g^{-1} up to 2 A g^{-1}. Table S2 in SI is reporting the discharge capacitance of the devices at the investigated current density, while Fig. 4 (a, b, c) is reporting the charge-discharge profiles of the devices at 0.1 A g^{-1} and 1 A g^{-1}. As shown, these devices display the expected shape (although not complety free of distortion) and, in accordance with the CV measurements, that containing HCOONa is the one displaying the most marked distortion from ideal behaviour, which is consistent with the most distorted CV observed in Fig. 3 for this electrolyte. Overall, the resistance of the devices appears low after cycling, 4 Ω, 8 Ω and 6 Ω for system containing 1 m HCOOLi in H_2O, 1 m HCOONa in H_2O and 1 m HCOOK in H_2O, respectively, as shown in Fig. S2 in SI. Figure S3 is comparing the energy and the power densities of the three devices in a Ragone plot. As shown, all devices display comparable performance. At 1 A g^{-1} the asymmetric SC containing 1 m HCOOK in H_2O displays a power and energy of 1.6 kW kg^{-1} and 8.8 Wh kg^{-1} (related to the total mass of active material), respectively. These values are comparable with those reported for devices with comparable operating voltage.

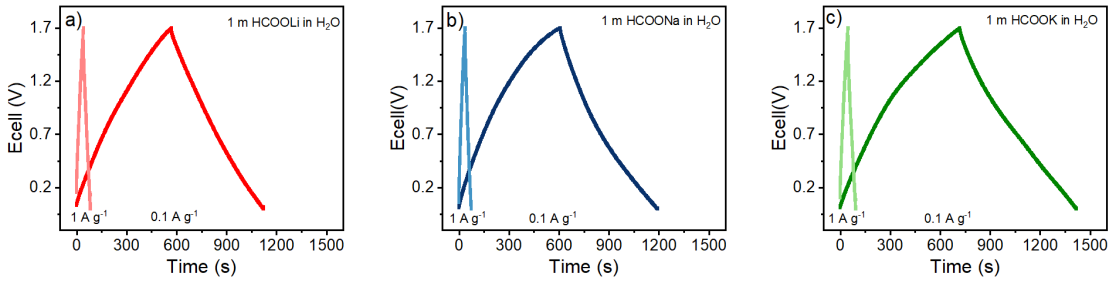

Figure 4. Voltage profile of the asymmetric Sc containing a) 1 m HCOOLi in H_2O;b) 1 m HCOONa in H_2O and c) 1 m HCOOK in H_2O

Finally, the cycling stability of these devices has been investigated carrying out 10,000 galvanostatic cycles at 1 A g^{-1} (using an operating voltage of 1.7 V). Figure 5 is

showing the variation of the capacitance of the devices through the cycling process (Fig. 5a, c, e) as well as the comparison of the 100th and 9999th voltage profiles of the cell, and potential of positive and negative electrodes. The initial capacitance of the full cell with 1 m HCOOK in H_2O is 32 F g^{-1} (referred to the total mass of active material in both sides of electrodes), which is a value comparable to that of the analogous devices reported in literature.[15-17] The capacitance retention after 10000 cycles of the devices containing 1 m HCOOLi in H_2O, 1 m HCOONa in H_2O and 1 m HCOOK in H_2O were 85%, 90% and 85%, respectively. As shown in Figures 5b, 5d and 5f during the cycling process a shift of the MnO_2 electrode towards higher potential is taking place, causing a decrease of the total capacitance of the device. Nonetheless, these results indicate that the use of formate-based electrolytes is making possible the realization of devices with high stability during prolonged charge-discharge tests. As indicated in Table S3 of the SI the cycling stability observed in all considered formate electrolytes is comparable with that of asymmetric SC based on commonly used aqueous electrolytes.

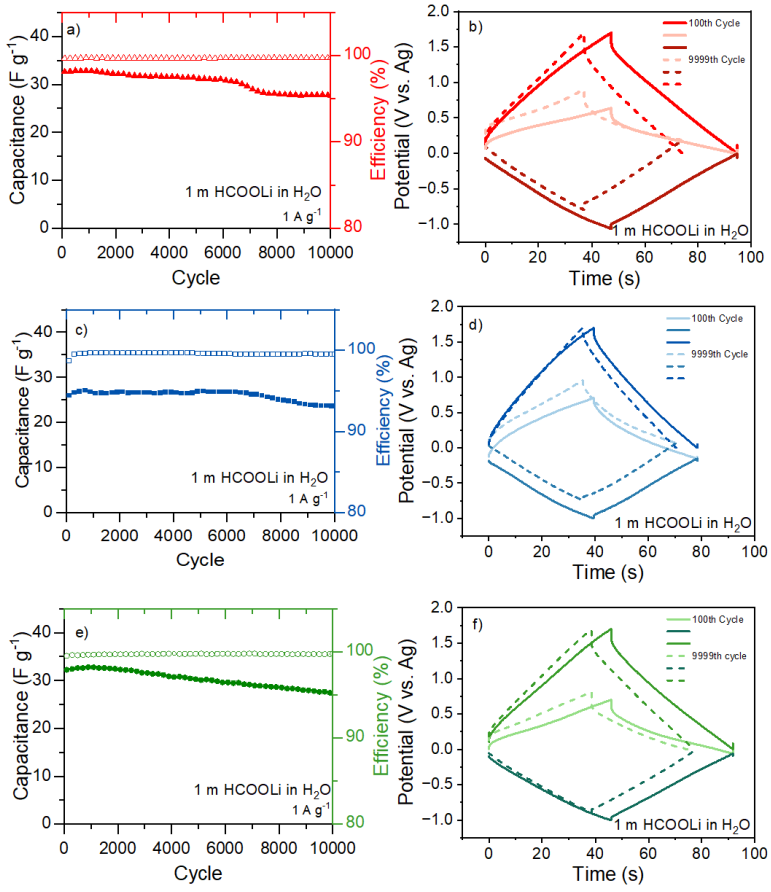

Figure 5: a) Cycling stability at 1 A g^{-1} of asymmetric SC containing 1 m HCOOLi in H_2O and b) Evolution of voltage profiles of the cell, positive and negative electrode during the cycling process. c) Cycling stability at 1 A g^{-1} of asymmetric SC containing 1 m HCOONa in H_2O and d) Evolution of voltage profiles of the cell, positive and negative electrode during the cycling process. e) Cycling stability at 1 A g^{-1} of asymmetric SC containing 1 m HCOOK in H_2O and f) Evolution of voltage profiles of the cell, positive and negative electrode during the cycling process.

Conclusion

In this work, we reported on the use of formate based aqueous electrolytes (1 m HCOOLi in H_2O, 1 m HCOONa in H_2O, and 1 m and HCOOK in H_2O) in asymmetric SC containing AC and MnO_2 electrodes. We showed that these cheap and non-toxic electrolytes display high conductivity and low viscosity. Their use makes possible the design of devices with operating voltage as high as 1.7 V. The asymmetric SC containing these electrolytes display promising values of capacitance, energy and power densities. Furthermore, they have shown high cycling stability over 10.000 cycles carried out at 1 A g^{-1}. Taking these results into account, the investigated formate based electrolytes can be considered as promising, low cost and environment friendly aqueous electrolytes suitable for the realization of high performance and low cost energy storage system.

Acknowledgements

SL and AB wish to thank the Bundesministerium für Wirtschaft und Energie (BMWi)-programm Zentrales Innovationsprogram Mittelstand (ZIM) within the project ZF4050709LT9 for financial support. CD and TB want to thank the ANR STORE-EX (ANR-10LABX-76-01) and the French network on electrochemical energy storage (RS2E). The authors also thank PRINCE Specialty Products LLC (610 Pittman Road, Baltimore, MD21226, USA) for supplying the provision of the MnO_2 SSA product.

References

1. IEA. IEA, Paris, 2023.
2. J. B. Goodenough and Y. Kim, *Chem. Mater.,* **22** (3), 587-603 (2010).
3. J. M. Tarascon and M. Armand, *Nature,* **414** (6861), 359-367 (2001).
4. P. Simon, Y. Gogotsi, and B. Dunn, *Science,* **343** (6176), 1210-1211 (2014).
5. J. R. Miller and P. Simon, *Science,* **321** (5889), 651-652 (2008).
6. F. Béguin, V. Presser, A. Balducci, and E. Frackowiak, *Adv. Mater.,* **26** (14), 2219-2251 (2014).
7. S. Hadži-Jordanov, H. Angerstein-Kozlowska, and B. E. Conway, *J. electroanal. chem. interfacial electrochem.,* **60** (3), 359-362 (1975).
8. J. P. Zheng and T. R. Jow, *J. Electrochem. Soc.,* **144** (7), 2417 (1997).
9. J. W. Long, K. E. Swider, C. I. Merzbacher, and D. R. Rolison, *Langmuir,* **15** (3), 780-785 (1999).
10. H. Y. Lee and J. B. Goodenough, *J. Solid State Chem.,* **144** (1), 220-223 (1999).
11. S. C. Pang, M. A. Anderson, and T. W. Chapman, *J. Electrochem. Soc.,* **147** (2), 444 (2000).
12. M. Toupin, T. Brousse, and D. Bélanger, *Chem. Mater.,* **16** (16), 3184-3190 (2004).
13. B. E. Conway, *Electrochemical supercapacitors: scientific fundamentals and technological applications*, Springer Science & Business Media (2013).

14. T. Brousse, D. Bélanger, and J. W. Long, *J. Electrochem. Soc.,* **162** (5), A5185-A5189 (2015).
15. M. S. Hong, S. H. Lee, and S. W. Kim, *Electrochem. Solid-State Lett.,* **5** (10), A227 (2002).
16. T. Brousse, M. Toupin, and D. Bélanger, *J. Electrochem. Soc.,* **151** (4), A614 (2004).
17. T. Brousse, P.-L. Taberna, O. Crosnier, R. Dugas, P. Guillemet, Y. Scudeller, Y. Zhou, F. Favier, D. Bélanger, and P. Simon, *J. Power Sources,* **173** (1), 633-641 (2007).
18. T. Brousse, M. Toupin, R. Dugas, L. Athouël, O. Crosnier, and D. Bélanger, *J. Electrochem. Soc.,* **153** (12), A2171 (2006).
19. O. Ghodbane, J.-L. Pascal, and F. Favier, *ACS Appl. Mater. Interfaces.,* **1** (5), 1130-1139 (2009).
20. S. Devaraj and N. Munichandraiah, *J. Phys. Chem. C,* **112** (11), 4406-4417 (2008).
21. H. A. Mosqueda, O. Crosnier, L. Athouël, Y. Dandeville, Y. Scudeller, P. Guillemet, D. M. Schleich, and T. Brousse, *Electrochim. Acta,* **55** (25), 7479-7483 (2010).
22. E. Eustache, C. Douard, A. Demortière, V. De Andrade, M. Brachet, J. Le Bideau, T. Brousse, and C. Lethien, *Adv. Mater. Technol.,* **2** (10), 1700126 (2017).
23. S. Liu, R. Klukas, T. Porada, K. Furda, A. M. Fernández, and A. Balducci, *J. Power Sources,* **541** 231657 (2022).
24. L. H. Hess and A. Balducci, *ChemSusChem,* **11** (12), 1919-1926 (2018).
25. L. H. Hess, L. Wittscher, and A. Balducci, *Phys. Chem. Chem. Phys.,* **21** (18), 9089-9097 (2019).
26. A. Balducci, R. Dugas, P. L. Taberna, P. Simon, D. Plée, M. Mastragostino, and S. Passerini, *J. Power Sources,* **165** (2), 922-927 (2007).
27. T. Stettner, P. Huang, M. Goktas, P. Adelhelm, and A. Balducci, *J. Chem. Phys.,* **148** (19), 193825 (2018).
28. J. Krummacher, C. Schütter, S. Passerini, and A. Balducci, *ChemElectroChem,* **4** (2), 353-361 (2017).
29. S. Liu, T. Stettner, R. Klukas, T. Porada, K. Furda, A. M. Fernández, and A. Balducci, *ChemElectroChem,* **9** (22), e202200711 (2022).
30. H. Avireddy, B. W. Byles, D. Pinto, J. M. Delgado Galindo, J. J. Biendicho, X. Wang, C. Flox, O. Crosnier, T. Brousse, E. Pomerantseva, J. R. Morante, and Y. Gogotsi, *Nano Energy,* **64** 103961 (2019).
31. J. W. Gittins, Y. Chen, S. Arnold, V. Augustyn, A. Balducci, T. Brousse, E. Frackowiak, P. Gómez-Romero, A. Kanwade, L. Köps, P. K. Jha, D. Lyu, M. Meo, D. Pandey, L. Pang, V. Presser, M. Rapisarda, D. Rueda-García, S. Saeed, P. M. Shirage, A. Ślesiński, F. Soavi, J. Thomas, M.-M. Titirici, H. Wang, Z. Xu, A. Yu, M. Zhang, and A. C. Forse, *J. Power Sources,* **585** 233637 (2023).
32. E. Frackowiak, Q. Abbas, and F. Béguin, *J. Energy Chem.,* **22** (2), 226-240 (2013).
33. Q. Gao, L. Demarconnay, E. Raymundo-Piñero, and F. Béguin, *Energy Environ Sci.,* **5** (11), 9611-9617 (2012).
34. A. Boisset, L. Athouël, J. Jacquemin, P. Porion, T. Brousse, and M. Anouti, *J. Phys. Chem. C,* **117** (15), 7408-7422 (2013).